*J. Fluid Mech.* (1989), *vol.* 208, *pp.* 395–415
*Printed in Great Britain*



# The distortion of short internal waves produced by a long wave, with application to ocean boundary mixing

By S. A. THORPE
Department of Oceanography, The University, Southampton SO9 5NH, UK

(Received 10 November 1988)

The propagation of a train of short, small-amplitude, internal waves through a long, finite-amplitude, two-dimensional, internal wave is studied. An exact solution of the equations of motion for a Boussinesq fluid of constant density gradient is used to describe the long wave, and its distortion of the density gradient as well as its velocity field are accounted for in determining the propagation characteristics of the short waves. To illustrate the magnitude of the effects on the short waves, particular numerical solutions are found for short waves generated by an idealized flow induced by a long wave adjacent to sloping, sinusoidal topography in the ocean, and the results are compared with a laboratory experiment. The theory predicts that the long wave produces considerably distortion of the short waves, changing their amplitudes, wavenumbers and propagation directions by large factors, and in a way which is generally consistent with, but not fully tested by, the observations. It is suggested that short internal waves generated by the interaction of relatively long waves with a rough sloping topography may contribute to the mixing observed near continental slopes.

## 1. Introduction

The distortion of short waves by those of larger scale has important consequences in the ocean. Short surface waves riding on longer waves can be severely modulated, leading to changes which may effect radar backscatter. Our purpose here is to investigate the modulation of short *internal* waves in a background dominated by a single long-wave component since this, for reasons which we shall later explain (§3), may have an important bearing on diapycnal mixing near ocean boundaries. The study parallels that of Longuet-Higgins (1987; see also Henyey *et al.* 1988) for the propagation of short waves on long surface gravity waves, with the advantage that we shall here begin with an exact solution for the long wave. The analysis is also similar to that of Broutman (1984, 1986), Broutman & Young (1986), and Broutman & Grimshaw (1988), who selected as the long wave an inertial wave or wave packet which, whilst producing a variable shear flow, induces no change in the density field through which the short waves are propagating. The analysis derived here may be seen as supplementing studies such as those of Müller & Karlsson (1981) in which short waves contribute to the instability of long waves, and more particularly, in its application to boundary mixing, to those of Baines (1971*a*, *b*) and Mied & Dugan (1976) who considered the reflexion of internal waves from rough topography.

## 2. Analysis

### 2.1. *The long wave*

An exact, two-dimensional internal wave solution to the equations of motion in a uniformly stratified (constant buoyancy frequency, $N_0$), non-diffusive, inviscid, Boussinesq fluid is

$$\psi = \frac{A\Sigma}{L}\sin\theta, \tag{1}$$

$$v = \frac{AfM}{L}\sin\theta, \tag{2}$$

where the velocity is $\boldsymbol{U} = (\partial\psi/\partial z, v, -\partial\psi/\partial x)$ and the density is

$$\rho = \rho_0\left(1 - \frac{N_0^2 z}{g} + \frac{N_0^2 A}{g}\sin\theta\right). \tag{3}$$

Here $g$ is the acceleration due to gravity, $L, M$ are the horizontal and vertical wavenumbers of the internal wave of amplitude $A$ and frequency $\Sigma$, $\theta = Lx + Mz - \Sigma t$, and $f$ is the Coriolis parameter. The dispersion relation is

$$\Sigma^2 = \frac{N_0^2 L^2 + f^2 M^2}{L^2 + M^2}. \tag{4}$$

The isopycnal displacements $\eta(x, z_0, t)$ are found by solving $\rho =$ constant on $z = z_0 + \eta(x, z_0, t)$;

$$\eta = A\sin(Lx + M(z_0 + \eta) - \Sigma t). \tag{5}$$

The lines of constant phase in the $(x, z)$-plane are given by $x\sin\alpha + z\cos\alpha =$ constant, where $L = K\sin\alpha$ and $M = K\cos\alpha$, and since $(\partial\psi/\partial z)\sin\alpha + (\partial\psi/\partial x)\cos\alpha = 0$, they are parallel to the particle motion. If we take new axes $X$ and $Z$ in the direction of the wave phase velocity and parallel to the wave crests respectively, then the motion is in the $Z$-direction, with particle speed $(-A\Sigma\sin\alpha)\cos(KX - \Sigma t)$ (see figure 1). The group velocity in the $(x, z)$-plane is

$$\boldsymbol{c}_G = \frac{(N_0^2 - f^2)}{\Sigma K^3}(\cos\alpha, 0, -\sin\alpha), \tag{6}$$

and is at right angles to the phase speed vector $\boldsymbol{c} = (\Sigma/K)(\sin\alpha, 0, \cos\alpha)$, but parallel to the particle motion.

The slope of isopycnal surfaces is given by

$$\frac{\partial\eta}{\partial x} = \frac{\phi\tan\alpha}{1-\phi}, \tag{7}$$

where $\phi = AM\cos\theta$, becoming vertical in part of the wave when $AM = r \geqslant 1$. The local buoyancy frequency $N_z$ is given by $N_z^2 = N_0^2(1-\phi)$ and an equivalent parameter relation for horizontal gradients, $N_x$, where $N_x^2 = -(g/\rho_0)\,\partial\rho/\partial x$, is given by

$$N_x^2 = -N_0^2\phi\tan\alpha.$$

The minimum Richardson number, $J = N_z^2/(\mathrm{curl}\,\boldsymbol{U})^2$, is

$$\cos^2\alpha/\{2[1-(1-r^2(1+\lambda))^{\frac{1}{2}}]\} \quad \text{if} \quad (1+\lambda) < 1/r,$$

or

$$\cos^2\alpha(1-r)/(\lambda r^2) \quad \text{if} \quad (1+\lambda) > 1/r,$$

where

$$\lambda = (f\cot\alpha/N_0)^2.$$

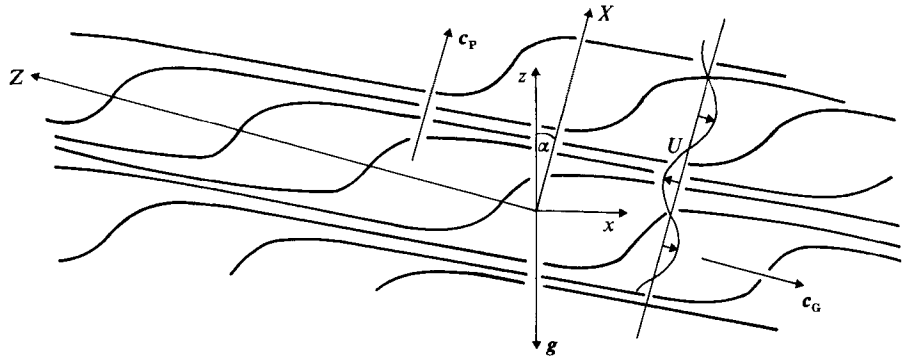


FIGURE 1. The notation used for long internal wave. The curves show surfaces of constant density.

The stability of the wave with $f = 0$ has been examined by Mied (1976), Drazin (1977) and Klostermeyer (1982) using Floquet theory. It is parametrically unstable even at small amplitude and so may be expected to break down at some distance from its generation site. Locally however (and we have in mind the region of ocean near the continental slope), it may provide a close approximation to the fluid at some (large) scale and we may usefully consider the propagation of relatively short and small-amplitude internal waves in the density and velocity field described by (1)–(3).

### 2.2. *The short waves*

The vertical acceleration produced by the long wave, $\partial^2\psi/\partial x\,\partial t$, is $A\Sigma^2\sin\theta$ and for oceanic internal waves, even with $A \sim 100$ m and $\Sigma \leqslant N_0 \sim 10^{-2}$ s$^{-1}$ this is very much less than $g$. In the examination of the short-wave modulation the effects of vertical acceleration are therefore neglected, in contrast to the comparable study of surface waves where they are paramount. We must, however, account for the long-wave-induced variation in the density field (3) through which the short waves are propagating. For values of $r$ near unity this variation is substantial.

The short waves are supposed to be of such small amplitude as to be linear, and of such small length that at any instant they effectively propagate within a uniform environment produced by the long wave. Provided that $J$ is sufficiently large (it must be $>\frac{1}{4}$), the local effects of the shear produced by the long waves may be neglected (Bretherton 1966; Bretherton & Garrett 1968; Booker & Bretherton 1967) and we need only account for the local density field. We consider therefore the propagation of waves in a uniformly stratified medium but having both horizontal and vertical variation in density $\rho_1$, such that $N_x^2 = -(g/\rho_0)(\partial\rho_1/\partial x)$ and $N_z^2 = -(g/\rho_0)(\partial\rho_1/\partial z)$ are constant.

The equations of motion may be solved to give a dispersion relation for the intrinsic wave frequency $\sigma$ as a function of wavenumber $(l, 0, n)$;

$$\sigma^2 = \frac{N_z^2 l^2 - N_x^2 ln + f^2 n^2}{(l^2 + n^2)}. \tag{8}$$

For simplicity we have chosen here to consider waves in the $(x, z)$-plane and to disregard those having a $y$-wavenumber (see the Appendix). As before, the phase and group velocities of these waves are at right angles, but the waves may be 'locally unstable' if $\sigma^2 < 0$. Writing $l = k\sin\beta, n = k\cos\beta$ we have

$$\sigma^2 = N_z^2\sin^2\beta - N_x^2\sin\beta\cos\beta + f^2\cos^2\beta. \tag{9}$$

It may be shown algebraically that $\sigma^2$ is bounded between the two values

$$\tfrac{1}{2}\{N_z^2+f^2\pm[(N_z^2-f^2)^2+N_x^4]^{\frac{1}{2}}\}.$$

The minimum value of $\sigma^2$ at $\beta=(\frac{1}{2})\tan^{-1}[N_x^2/(N_z^2-f^2)]$ is negative if $N_x^4>4f^2N_z^2$, or, using the expressions for $N_x$ and $N_z$ in terms of $\phi$ (see §2.1), when $\phi^2>4\lambda(1-\phi)$. A necessary condition for instability is thus

$$r^2>4\lambda(1-r). \tag{10}$$

Physically the instability corresponds to a disturbance along a direction between the horizontal and that of the mean long-wave isopycnals, which slope at an angle $\tan^{-1}(N_x^2/N_z^2)$. It carries denser fluid downwards and light fluid upwards, thus locally reducing the potential energy. Rotation (larger $\lambda$) tends to stabilize the instability.

The energy of the waves can be estimated by taking the scalar product of the velocity components $(u,v,w)$ and a density perturbation term with their respective equations of motion and conservation of density in the usual way (see for example Gill 1982, section 6.7), and adding to give

$$\frac{\partial}{\partial t}\left\{\tfrac{1}{2}(u^2+v^2+w^2)-\frac{g^2\rho^2}{2\rho_0^2N_z^2}\right\}+\frac{g\rho uN_x^2}{N_z^2}+\left[\frac{1}{\rho_0}\frac{\partial}{\partial x}(pu)+\frac{1}{\rho_0}\frac{\partial}{\partial z}(pw)\right]=0. \tag{11}$$

The terms in the square bracket represent the rate at which work is done by the pressure, $p$. Using the linear solution for

$$u=u_0\cos(lx+nz-\sigma t)$$

and for the density perturbation

$$\rho=(u_0/n\sigma)(lN_x^2-nN_z^2)(\rho_0/g)$$

to provide an expression for $\rho u$ we find, correct to second order,

$$\frac{\partial}{\partial t}\left\{\tfrac{1}{2}\left[(u^2+v^2+w^2)+\frac{g\rho^2}{\rho_0^2(N_z^2-N_x^2\cot^2\beta)}\right]\right\}+\left[\frac{1}{\rho_0}\frac{\partial}{\partial x}(pu)+\frac{1}{\rho_0}\frac{\partial}{\partial z}(pw)\right]=0. \tag{12}$$

The energy density of the waves, $E$, is now given by the expression within the curly brackets, and this can be evaluated using the linear solution of the equations of motion to give a second-order expression

$$E=\frac{\rho_0a^2\sigma^2N_z^2}{2(N_z^2\sin\beta-N_x^2\cos\beta)^2}, \tag{13}$$

where $a$ is the amplitude of the short waves. (Except for the term in $N_x$, this has precisely the same form as that given by Gill (1982, equation (8.6.5)).) The ratio of kinetic to potential energy is unchanged from that given by Gill in his equation (8.6.6).

The component of group velocity in the direction of phase propagation of the long waves, parallel to the $X$-axis, is

$$c_{gX}=\frac{\partial\sigma}{\partial l}\sin\alpha+\frac{\partial\sigma}{\partial n}\cos\alpha,$$

which, after some algebra, becomes

$$c_{gX}=\frac{\sin(\alpha-\beta)}{2\sigma k}[(N_z^2-f^2)\sin2\beta-N_x^2\cos2\beta]. \tag{14}$$

Three conservation equations are formulated to describe the propagation of the short waves. We assume first that there is uniformity in the $Z$-direction parallel to the long-wave crests, recalling also that the long-wave particle speed is independent of $Z$. The component of wavenumber parallel to the crests of the long waves is therefore conserved;

$$l\cos\alpha - n\sin\alpha = c_1, \quad \text{constant}. \tag{15}$$

Secondly wave phase is conserved, so that the absolute frequency of the short waves is constant in a frame of reference moving with the long waves. Recalling that the long waves move at speed $\Sigma/K$ in direction $X$ and that the particle motions are at right angles with speed $(-A\Sigma\sin\alpha)\cos KX$ in the $Z$-direction, in the frame of reference moving with the long waves we have

$$\sigma - (\Sigma/K)(l\sin\alpha + n\cos\alpha) + (n\sin\alpha - l\cos\alpha)\frac{A\Sigma}{\sin\alpha}\cos KX = c_2, \quad \text{constant}. \tag{16}$$

The third equation describes conservation of wave action, $E/\sigma$ (Garrett 1967). In the steady flow relative to a frame of reference moving with the long wave, the wave action does not change in time, so that, recalling uniformity in the $Z$-direction,

$$\frac{\partial}{\partial X}\left(\frac{\Sigma}{K} - c_{gX}\right)\frac{E}{\sigma} = 0, \tag{17}$$

and so the wave-action flux is constant:

$$\left(\frac{\Sigma}{K} - c_{gX}\right)\frac{E}{\sigma} = c_3, \quad \text{constant}. \tag{18}$$

The equations are non-dimensionalized by taking

$$\gamma = k/K, \quad s = \sigma/\Sigma. \tag{19}$$

The constants $c_1$, $c_2$ and $c_3$ are found by specifying $\gamma$, $s$, $\beta$ and $a$ at some reference position of $X$ ($\gamma_0, s_0, \beta_0$ and $a_0$ say) when $\phi, = AM\cos KX, = \phi_0$. The equations become

wavenumber:
$$\gamma\sin(\beta-\alpha) = C_1; \tag{20}$$

phase conservation:
$$s - \gamma\cos(\beta-\alpha) + \frac{\phi\gamma\sin(\beta-\alpha)}{\sin\sigma\cos\alpha} = C_2; \tag{21}$$

wave-action flux:

$$\left(\frac{a}{a_0}\right)^2(1-\phi)^2$$

$$\times\frac{\{\sin(\beta-\alpha)[(1-\phi-\lambda\tan^2\alpha)\sin 2\beta + \phi\tan\alpha\cos 2\beta] + 2s\gamma(1+\lambda)\sin^2\alpha\}}{4\gamma(1+\lambda)\sin\alpha[(1-\phi)\sin\beta + \phi\tan\alpha\cos 2\beta]^2} = C_3, \tag{22}$$

with the dispersion relation:

$$s^2 = \frac{\{\sin\beta[(1-\phi)\sin\beta + \phi\tan\alpha\cos\beta] + \lambda\tan^2\alpha\cos^2\beta\}}{(1+\lambda)\sin^2\alpha}, \tag{23}$$

where $C_1$, $C_2$ and $C_3$ correspond to $c_1$, $c_2$ and $c_3$ in the non-dimensional equations. We may eliminate $\gamma$ by substituting from (20) into (21) to give

$$s = C_2 + C_1\left(\cot(\beta-\alpha) - \frac{\phi}{\sin\alpha\cos\alpha}\right), \tag{24}$$

and using this to eliminate $s$ in (23), we have a quadratic equation for $\phi$ which has two roots, each a function of $\beta$. Numerical solutions may now be generated by choosing $\beta$, solving the quadratic for $\phi$, and then using (20) and (21) to find $\gamma$ and $s$ respectively. Roots with $|\phi| > r$, $\gamma < 0$ or $s < 0$ are discarded as being unrealistic. (We require $k$, $K$, $\sigma$ and $\Sigma$ to be greater than zero.) Equation (22) now gives values of $(a/a_0)^2$ which are $>0$ provided that $(\Sigma/K - c_{gX})$ does not change sign between reference position and the position at which the solution is to be found. Changes in sign occur at positions where the short waves are unable to propagate through the long wave. These correspond to the caustics discussed and analysed by Broutman (1986). (To the approximation considered here, the wave amplitude increases indefinitely as the caustics are approached. Broutman has described a local solution which avoids the singularity.)

We might illustrate the solutions by arbitrarily specifying conditions at the reference position. Having in mind a specific application, we have instead chosen to seek solutions that apply to short waves generated by the long-wave flow over topography. Whilst we express some reservations about the validity of this approach, the procedure does at least provide some illustrations in §4 which demonstrate the large effects which long waves may have on short waves.

## 3. Application

### 3.1. *Boundary mixing in the ocean*

It was suggested by Munk (1966), and later by Armi (1979), that mixing on ocean boundaries might be important in supporting the net diapycnal diffusion in deep water within ocean basins. The principal mechanism of mixing is, however, unknown. Whilst there exist mechanisms that may lead to the occurrence of unstable stratification in a viscous Ekman-type boundary layer driven by flow near a slope (see Weatherley & Martin 1978; Thorpe 1987*b*), there are also inviscid modes of instability associated with internal waves which might lead to turbulent diffusion. Eriksen (1982, 1985) has pointed to the possible importance of internal wave breaking on slopes with an inclination to the horizontal, $\delta$, which matches that of the characteristic propagation direction of the waves; that is at 'critical' frequencies, $\sigma_c$, where

$$\sigma_c^2 = N_0^2 \sin^2\delta + f^2 \cos^2\delta.$$

Cacchione & Wunsch (1974) observed instability near slopes for waves having this frequency in laboratory experiments and, in recent further experiments, G. N. Ivey (private communication) has found that turbulence sets in at sufficiently high Reynolds numbers. Thorpe (1987*a*) has shown that wave breaking might also occur at slopes other than the critical when the incident wave interacts resonantly with its *phase-locked* reflected wave. The estimated dissipation rates in the ocean appear sufficient to contribute a significant fraction of that across whole ocean basins (Garrett & Gilbert 1988).

Observations near 3300 m depth on the west slope of the Porcupine Bank south-west of Eire (Thorpe 1987*b*) show the presence of motions dominated by fluctuations at the period of the semi-diurnal, of $M_2$, tide with a strong baroclinic component which severely modulates the local density gradient. The wave appears to propagate in a plane roughly normal to the contours of the slope. The amplitude of the fluctuations reaches 60 m and the vertical density gradient measured over 100 m scales varies by factors of order 8:1, relatively weak gradients being found when the current is up-slope. The vertical wavelength of the waves is about 1000 m. The local

slope of the seabed in the area is about 3°, rather less than that of the wave characteristics (about 6°) and, whilst 'critical' conditions or those for resonant interactions are approached, they are not matched precisely (Thorpe 1988). Nevertheless the amplitude of the reflected wave, which in a linear inviscid model would increase indefinitely as critical conditions are approached, appears to greatly exceed that of the incident wave (as, for example, in the experiments of Thorpe & Haines 1987), and the motion is primarily determined by the reflected component.

Measurements in the lower 130 m of the water column made to a resolution of 0.1 mK at 20 s sampling rate (well below the mean local buoyancy period of about 2 hours) show a highly variable temperature structure within the $M_2$ oscillation. During the last 3 hours of rising isotherms (up-slope current), high-frequency oscillations have an amplitude of 10–12 m, whilst during the period of falling isotherms the corresponding amplitude is about 1 m (Thorpe 1987*b*, figure 22). Coherent 'layers' in the bottom 80 m with temperature gradients some 3–10 times greater than average have a vertical separation of 2–50 m, and show a notable downward trend as the isotherms rise (Thorpe 1987*b*, figure 23). Between these stable layers are observed statically unstable regions in which the potential density decreases with depth over scales of 10–20 m for short periods. An estimate of the rates of production of turbulent kinetic energy show that turbulence resulting from the observed 'inversions' may be comparable with, or even greater than, that produced by the shear stress on the seabed.

The observations reveal a situation in which significant mixing is being produced by large baroclinic motions. The downward-propagating layers suggest the presence of internal waves with downward phase speed and thus having an associated upward propagation of wave energy (Lazier 1973), and hence to a source of the waves on the seabed, although as we shall see later this interpretation may be too simplistic. There are at least two possible explanations for the absence of these waves. They may be bottom reflected, and enhanced, components of waves propagating downwards from the 'spectrum' of waves existing in the overlaying ocean. Alternatively, they may result from the local topographic generation of small-scale waves (i.e. 20–50 m vertical wavelength) by the large-scale, $M_2$, 1000 m vertical wavelength, baroclinic wave (see Bell 1975), which subsequently so distorts the short waves as to induce their breaking. It is this latter idea that we shall pursue here. We are strongly motivated by the laboratory experiments of Koop (1981; see especially figure 22) and Koop & McGee (1986; see especially figure 14), which shows the onset of breaking in short waves induced by the motion of shear flow over topography, as well as by other experiments of wave intensification in accelerating shear flows at lower Reynolds number (Thorpe 1984).

Our conceptual model of the mixing is thus one in which large waves interact with topography, producing small-scale waves which are then forced to break as they are distorted by the large-scale modulations.

### 3.2. *Waves generated by interaction of the long wave with bottom topography*

We assume, for simplicity, that the near-bottom long waves like those observed on the Porcupine Bank are dominated by a single-frequency component. We envisage a situation in which, although the total long-wave field near the slope may more exactly be described by the superposition of an incident and a reflected wave, conditions are close to critical so that the amplitude of the reflected wave is much greater than that of the incident wave, and the motion and density are adequately accounted for by the reflected wave alone. (The field of density and motion within

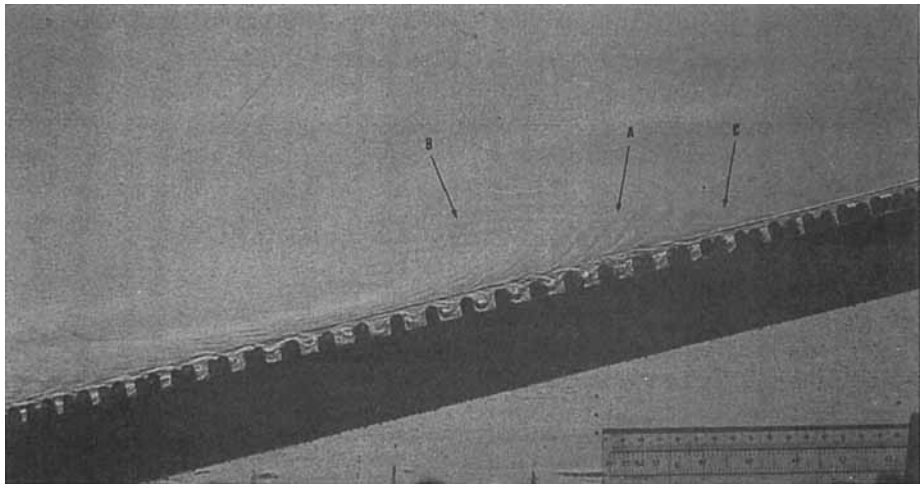


FIGURE 2. Shadowgraph of the laboratory experiment. For easy comparison with the theory, the negative has been printed back to front so that the long internal waves appear to approach the slope (to which are fixed square horizontal bars separated at 1.9 cm intervals) from the left. They produce a flow over the bars which generate the short waves which can be seen at A, B and C.

the incident and reflected waves cannot be described simply by their superposition, since although each may be an exact solution of the equation of motion, they interact; see Thorpe (1987*a*). A finite-amplitude formulation of the wave field is thus not a simple matter.) We shall moreover ignore the restriction to the flow imposed by the presence of the slope, so that, even in its vicinity, the assumption of $Z$-independence, essential in formulating (15) and (17), is retained. These assumptions allow us to specify initial conditions for the short waves and to illustrate the theory developed in §2.2. Our objective here is to provide a *qualitative* description based on the understanding developed in earlier sections, which may help to interpret observations. It would be appropriate to consider at a later stage the effect of approximating the long-wave field by a superposition of incident and reflected waves, whilst then acknowledging that finite-amplitude effects may not be adequately included. It should be recalled, however, that in reality, with which we have ultimately to cope, there are other more serious effects that we have ignored such as the non-uniformity of the slope and density gradients, or the fact that the field of motion is broad-band. The shortcomings of the assumptions are discussed further in §5 when we come to the application of the results.

We consider a plane source of short waves which is inclined on a slope at an angle $\delta$ to the horizontal with wavenumber $k_1$. For illustration, an experiment was done in a 20.5 cm wide, 27.3 cm deep, channel filled with a stratified brine solution having a constant density gradient. Waves of the second vertical mode are generated at one end of the channel and propagate towards a uniform rigid slope at 15° to the horizontal on which lies a grid of horizontal square bars. The bars are 0.6 cm square and are at 1.9 cm centre-to-centre separation giving a wavenumber $k_1 = 3.31$ cm$^{-1}$. (The grid was constructed for an experiment in which it is rapidly oscillated to produce turbulence, but in the present experiments it is held stationary.)

Figure 2 shows a shadowgraph image taken shortly after the arrival of a train of internal waves with $\alpha = 150°$, coming from the left. The waves reflect up the slope as described by Cacchione & Wunsch (1974) and Thorpe & Haines (1987). The

incident wavelength is $\lambda_I = 27.3 \times \cos 30° = 23.6$ cm, whilst the (dominant) reflected wavelength $\lambda_R = \lambda_I \sin(\alpha-\delta)/\sin(\alpha+\delta) = 8.6$ cm so that, for this wave, the bar spacing gives $k_1 = 4.55K$.

Small-scale waves are generated by the flow over the bars. Those most clearly visible in the shadowgraph are at A and B. These small-scale waves are generated as stationary waves on the plane with phase speed parallel to the slope and relative to the fluid

$$c = \frac{\sigma}{k_1} = V(t), \tag{25}$$

where $\sigma$ is the their intrinsic frequency and $V$ is the local up-slope current produced by the large-scale wave. If the waves travel at an angle $\beta$ to the horizontal then, by simple geometry, their wavenumber $k$ is given by

$$k = \frac{k_1}{\sin(\beta-\delta)}, \tag{26}$$

and, using the dispersion relation (9) to replace $\sigma$,

$$N_z^2 \sin^2\beta - N_x^2 \sin\beta\cos\beta + f^2\cos^2\beta = k_1^2 V^2. \tag{27}$$

$V$ is taken as the local component of the long-wave current parallel to the slope;

$$V = -(A\Sigma/\sin\alpha)\cos\Sigma t\cos(\alpha-\delta).$$

Using the earlier parameterization, (27) can be rewritten as a quadratic in $\tan\beta$:

$$(1-\phi-q)\tan^2\beta + \phi\tan\alpha\tan\beta + (\lambda\tan^2\alpha - q) = 0, \tag{28}$$

where $$q = \phi^2\cos^2(\alpha-\delta)\gamma_1^2(1+\lambda)/\cos^2\alpha, \quad \gamma_1 = k_1/K.$$

Given values of $\gamma_1$, the ratio of the length of the long wave to the wavelength of the slope topography, and of $\phi = \phi_0$, it is now possible to solve this quadratic and find real values (when they exist) of $\beta = \beta_0$ which satisfy the condition that the phase speed of the waves opposes the direction of $V$ and their group velocity is appropriately directed upwards *away* from the source plane. The values of $\beta_0$ are then restricted in $\pi < \beta_0 < \frac{3}{2}\pi$ for $\phi_0 > 0$ (up-slope flow) and

$$\tfrac{1}{2}\pi < \beta_0 < \pi-\delta \text{ or } 2\pi-\delta < \beta_0 < 2\pi$$

for $\phi_0 < 0$ (down-slope flow) with $\frac{1}{2}\pi < \alpha < \pi$, as shown in figure 3 (*a*, *b*). These values of $\phi_0$, $\beta_0$ and $\gamma_0$ (given by $\gamma_0 = \gamma_1/\sin(\beta_0-\delta)$ from equation (26)), are now used as the initial values to determine the constants in (20)–(22), and the analysis developed in §2.2 determines the phase configuration of the short waves within the long-wave field.

Since $\sigma$ has a bounded range of values, there is only a limited range of values $V$ for which solutions of (27) are possible; waves are thus generated only in particular parts of the 'ebb' and 'flood' cycle of the long wave. There are indeed discrete generation periods on either side of 'slack water' ($V = 0$) which may be reached either in an increasing or decreasing net flow.

The distance that waves travel away from the slope, $d$, may be estimated by calculating

$$d = \int_0^t c_{g1}\,\mathrm{d}t$$

(where $t$ is the time from the moment of their generation and $c_{g1}$ is the component of group velocity of the waves normal to the slope). This may be transformed to an

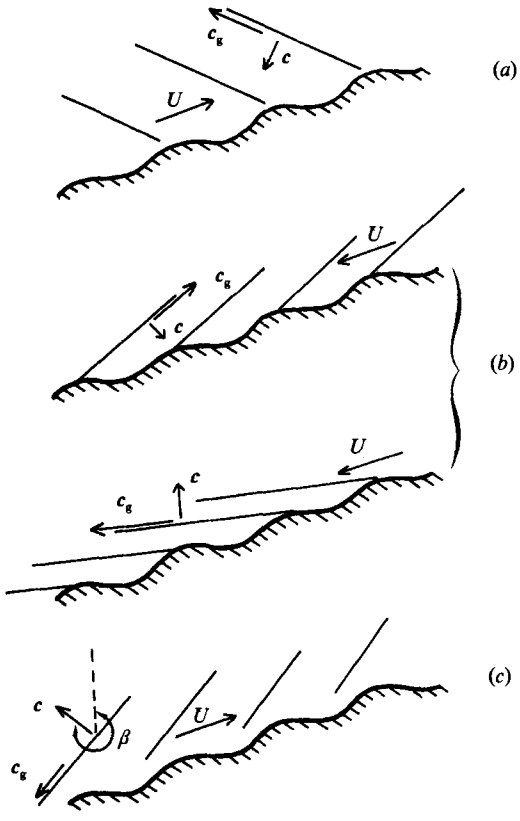


FIGURE 3. Generation of short waves with phase velocity $c$ and group velocity $c_g$ by flow over the sinusoidal slope: (*a*) up-slope flow $\phi > 0$; (*b*) down-slope flow $\phi < 0$, with waves possible in two quadrants; (*c*) shows how $\beta$ is measured. Here waves with $\frac{3}{2}\pi < \beta < 2\pi$ are being advected by an up-slope mean flow exceeding the down-slope component of phase speed (see §5).

integral over $\phi$ by noting that the phase position of the short waves in the long wave changes by $K(c-c_{gX})\,\mathrm{d}t$ in time $\mathrm{d}t$:

$$\mathrm{d}\phi = AM(\sin KX)K(c-c_{gX})\,\mathrm{d}t$$

so that

$$Kd = \pm\int \frac{c_{g1}\,\mathrm{d}\phi}{(c-c_{gX})(r^2-\phi^2)^{\frac{1}{2}}}, \tag{29}$$

where the sign is chosen so that $d$ increases for small departures of $\phi$ from $\phi_0$ (i.e. so that initially waves propagate away from the slope). In practice the integral was estimated by a finite-difference summation.

## 4. Results

The results are presented as a series of graphs in the $(\phi, \beta)$-space, showing first the orientation of waves $\beta$ as a function of $\phi = r\cos\theta$ which, since $\phi = 1-N_x^2/N_0^2$, is a measure of the variation of static stability in the long wave as the phase, $\theta$, changes.

We have chosen $r\,(=AM)$ as 0.8, a large value which, however, corresponds to those estimated both for the waves in the laboratory experiments and the largest waves observed off the Porcupine Bank.

Figures 4 and 5 use values appropriate to the Porcupine Bank. We take $\alpha = 174°$, $\delta = 3°$ and $\lambda = 0.9$, corresponding to $f/N_0 = 0.1$. Equation (10) then shows that the short-wave disturbances are stable. The minimum Richardson number in the long wave, $J = 0.34 > \frac{1}{4}$ and the maximum wave steepness (from (7)) is 22.8°. The wavelength of the long waves is about 1000 m, but an appropriate value of $\gamma_1$ is not well defined by the observations. We have taken the wavelength of the bottom topography as 250 m and 125 m (giving $\gamma_1 = 4$ and 8 respectively) for illustration.

Figure 4(*a*) shows the variation of $\beta$ with $\phi$ for $\gamma_1 = 4$. Waves are generated at the points marked by circles in either an increasing or decreasing up-slope flow ($\phi > 0$, and increasing or decreasing), or in an increasing or decreasing down-slope flow ($\phi < 0$, and decreasing or increasing, respectively), and are rotated in the changing shear and density field of the long wave. Waves generated during the periods of up-slope flow ($\phi_0 > 0, \beta_0 > \pi$) rotate clockwise for increasing $\phi$, or anticlockwise ($\beta$ decreasing to near $\pi$; waves with near-horizontal phase surfaces) as $\phi$ decreases. Waves generated in the down-slope flow ($\phi_0 < 0, \beta_0 < \pi$) are similarly rotated, but those carried below $\beta = \frac{1}{2}\pi$ may propagate into a 'caustic' zone where their group speed matches that of the long wave. As shown in figure 4(*b*), their amplitude increases considerably as the caustic is approached. Considerable amplification is found in the waves carried towards $\phi = 0.8$, especially those generated during the up-slope flow ($\beta > \pi$). We do not, however, find that these decrease the stability of the flow by significantly enhancing the shear. So as to indicate the effect of the shear produced by the short waves, figure 4(*c*) shows contours of a ratio $R_i' = J'/J_0$, where $J'$ is a local minimum-gradient Richardson number induced by the short waves and $J_0$ is its value at $(\beta_0, \phi_0)$. Here $J'$ is defined as the square of the ratio of the local buoyancy frequency to the $y$-component of the vorticity induced by the short waves. (An estimate of the local Richardson number based on the *total* vorticity of the flow – long and short waves together – requires a specification of the relative amplitudes of waves.) The Richardson number is most reduced by waves approaching $\beta = 0$, $\pi$ or $2\pi$, where their wavelength becomes small ($\gamma$ large, see figure 4*d*), or near the caustic. The condition that $\gamma$ should be large is not well satisfied for all the waves, although $\gamma > 3$ everywhere. The condition $\gamma \gg 1$ is, however, better satisfied for $\gamma_1 = 8$, shown in figure 5. The same general features can be seen, especially the large amplitudes reached near $\phi = 0.8$, for waves generated in the up-slope flow (figure 5*b*) and the small values of $R_i'$ near $\beta = 0$, $\pi$ and $2\pi$ (figure 5*c*), with the exception that no caustic develops and all waves survive throughout the range of $\phi$. Since $\phi$ is scaled with $r\,(=AM)$, results for smaller values of the long-wave amplitude, $A$, can be deduced simply by using the figures 4 and 5 with a revised maximum value of $\phi$. It may hence be seen, for example, that no caustic will be encountered for waves with $\gamma_1 = 4$ provided that $r < 0.46$. Using (29) we find that waves approaching the caustic in figure 4(*a*) have typically propagated a distance, $d$, of about 25 m off the seabed, whilst those formed in the up-slope flow ($\phi_0 > 0$) have travelled some 20 m by the time they arrive at $\phi = 0.8$.

Figure 6 applies to values appropriate to the laboratory experiments, namely $\alpha = 150°$, $\delta = 15°$, $\gamma_1 = 4.55$ and $\lambda = 0$ (since $f = 0$). The maximum isopycnal slope is (from (7)) 66.5°, and $J = 0.62$, $> \frac{1}{4}$. Conditions of 'instability', (10), are possible within the ranges of $\phi$ and $\beta$ shown as shaded areas in figure 6. No evidence is found that caustics are encountered by waves generated by the grid, assuming that the disturbances produced can accurately be described as waves with an up-slope wavelength equal to the bar spacing. Waves produced during the up-slope flow ($\phi_0 > 0, \beta_0 > \pi$) may promote instability as they reach $\beta = \pi$ as $\phi$ decreases below zero

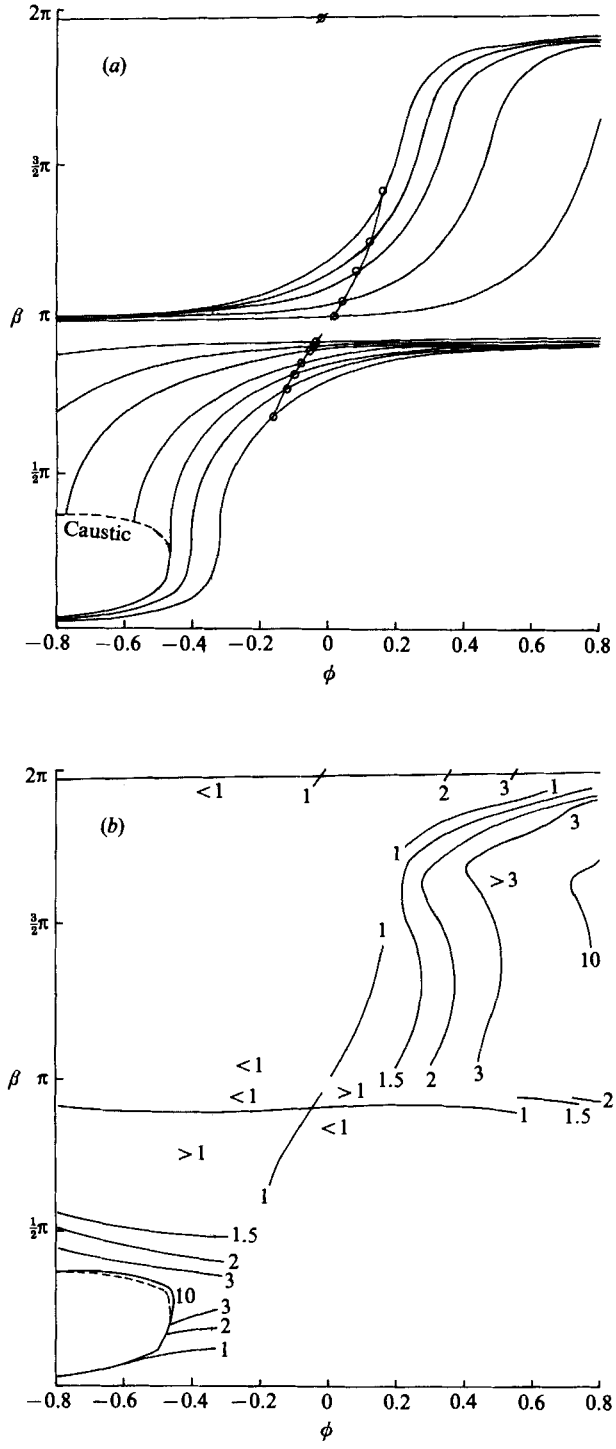


FIGURE 4 (*a*, *b*). For caption see facing page.

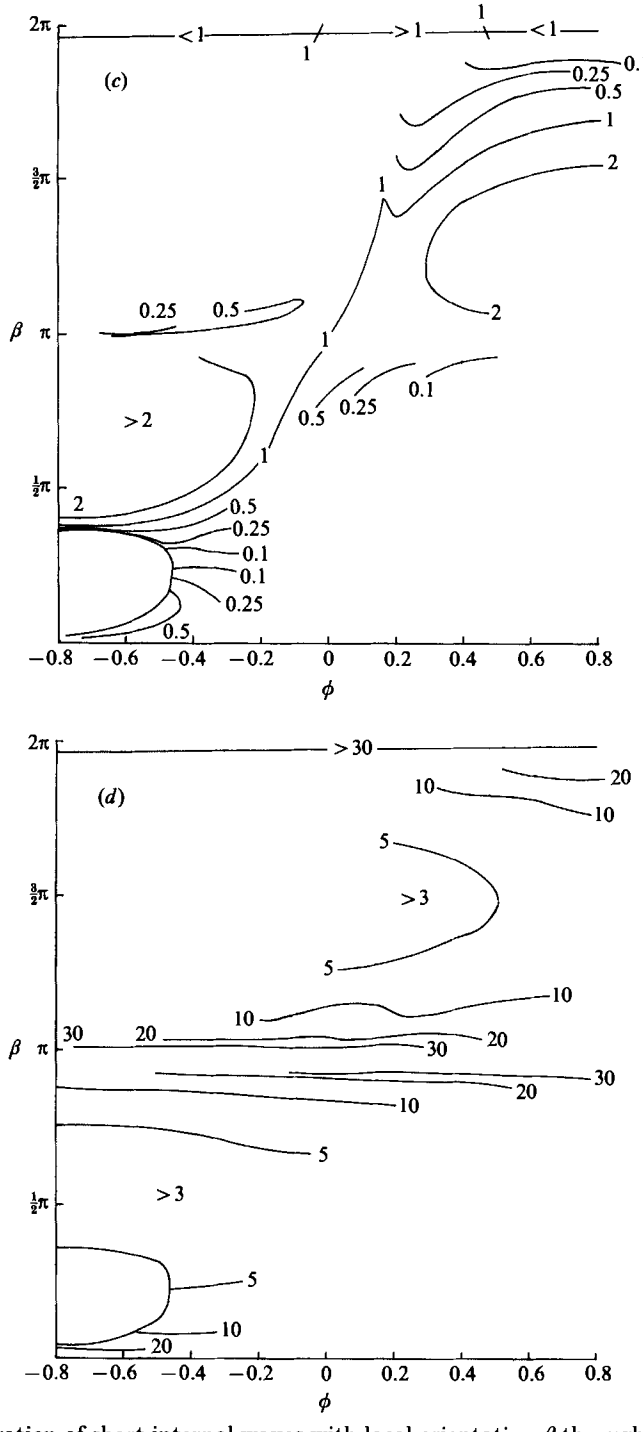


FIGURE 4. Propagation of short internal waves with local orientation $\beta$ through a long wave given by $\phi = AM\cos\theta$. The long wave travels at angle $\alpha = 174°$ to the vertical (see figure 1), and $f/N_0 = 0.1$. The short waves are generated by the current produced by the long wave on a slope inclined at an angle $\delta = 3°$ to the horizontal with a wavelength which is 0.25 times that of the long wave ($\gamma_1 = 4$). (*a*) The variation of $\beta$ with $\phi$. The short waves are generated at the points marked by circles. The curve labelled 'caustic' marks the locus of points where the group velocity of the short waves matches the phase speed of the long wave. (*b*) Contours of $a/a_0$, the amplification factor of the short waves. (c) Contours of $R_i'$, a measure of the local short-wave-induced Richardson number. (*d*) Contours of $\gamma$, the ratio of the long wave to short wave length.

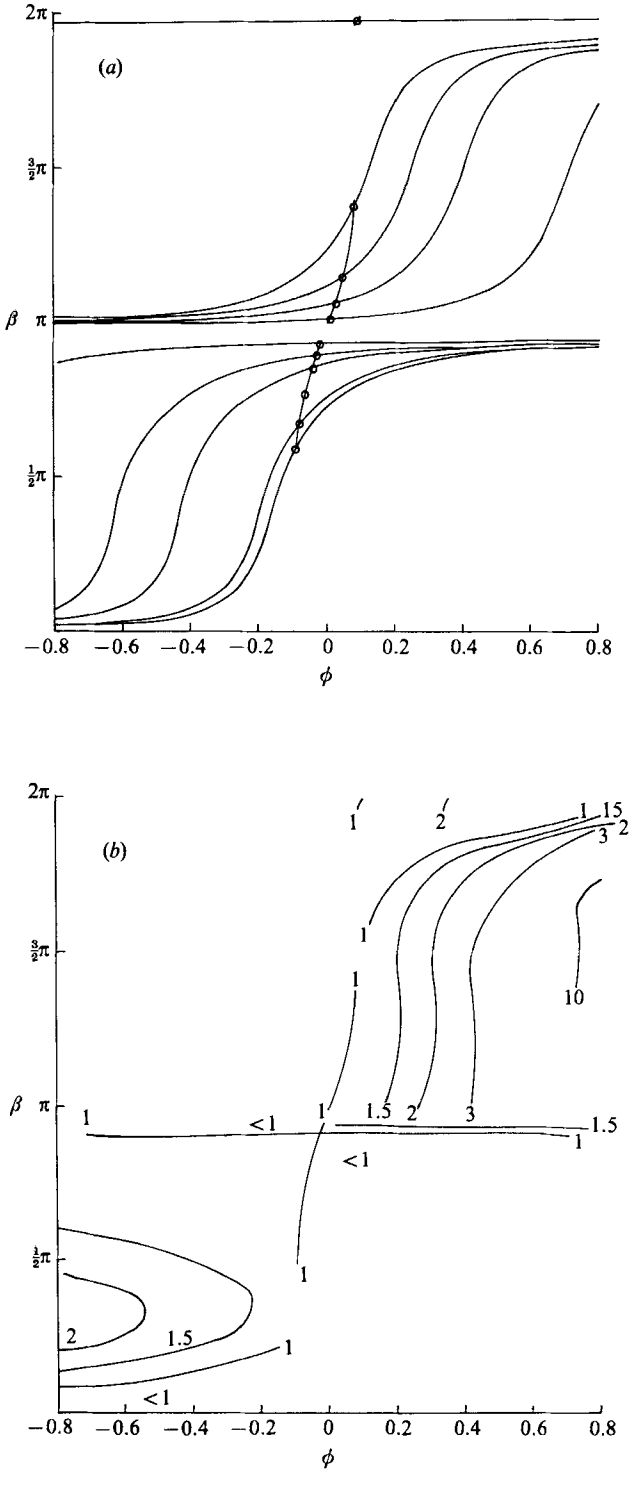


FIGURE 5(*a*, *b*). For caption see facing page.

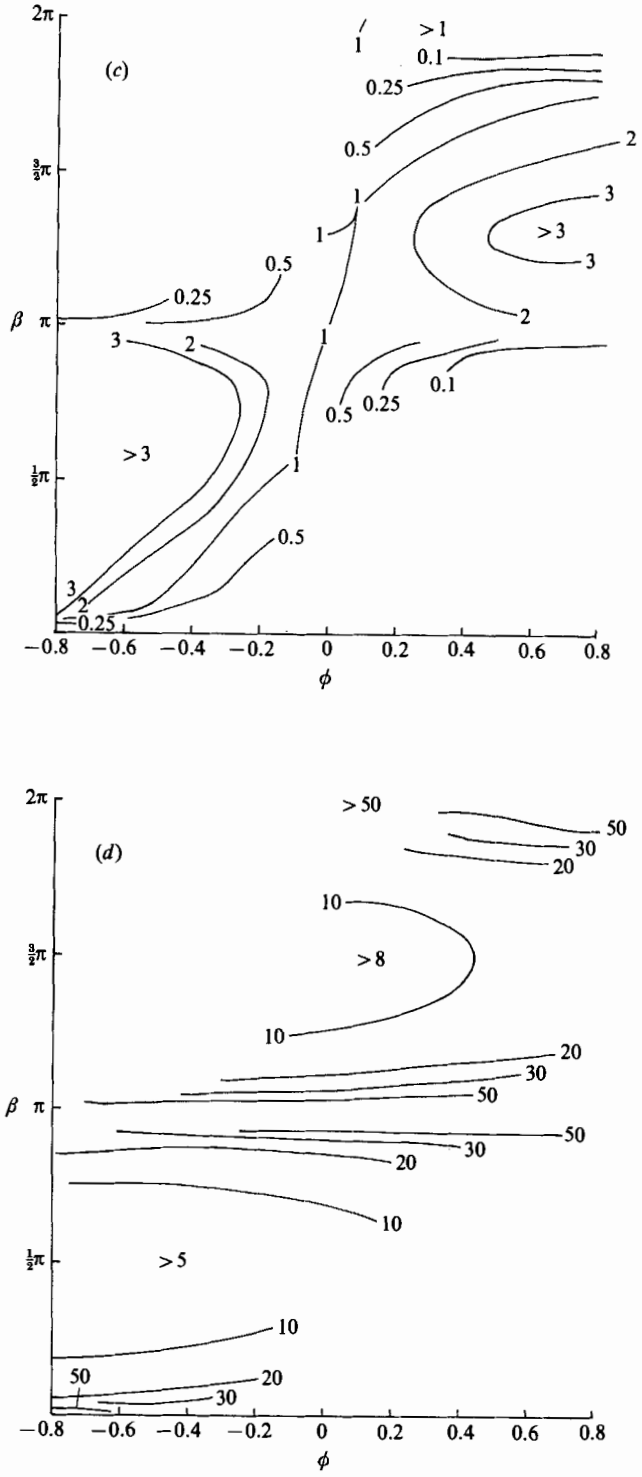


FIGURE 5. As for figure 4, but with $\gamma_1 = 8$. No 'caustic' develops in these conditions.

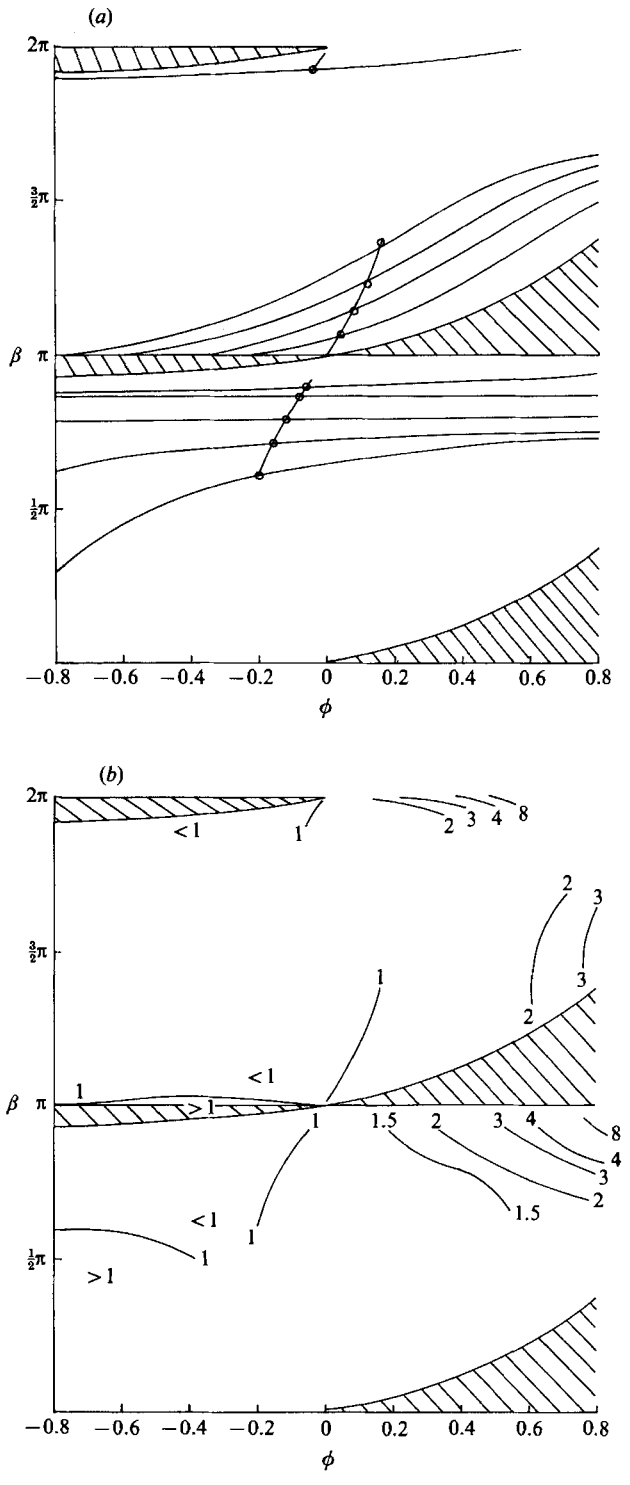


FIGURE 6(*a*, *b*). For caption see facing page.

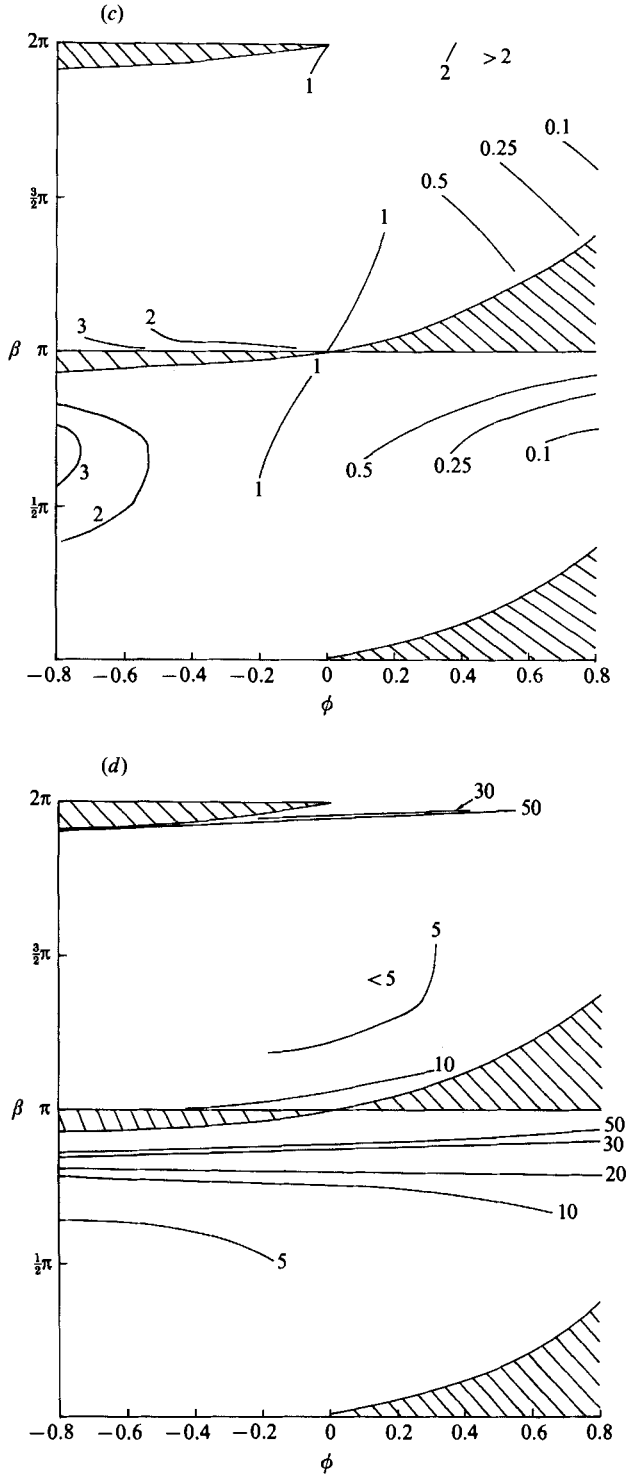


FIGURE 6. As for figure 4, but with values corresponding to the laboratory experiment, $\alpha = 150°$, $f/N_0 = 0$, $\delta = 15°$ and $\gamma_1 = 4.55$. No caustic develops, but there are regions (shaded) in which short waves are unstable.

(on a downward flow; figure 6*a*). From (9) it appears that the growth rate of the instability is unlikely to be large. The waves are not significantly amplified as they approach the unstable region (figure 5*b*). The greatest amplification occurs for $\phi$ near 0.8 and $\beta$ near $2\pi$, or where $\frac{3}{4}\pi < \beta < \pi$, with amplification factors exceeding 4 for $145° < \beta < 180°$. Large values also occur near $\beta = \frac{3}{2}\pi$, where $R_i'$ (figure 6*c*) is also small. Near ($\beta = \pi, \phi < 0$) and ($\beta = 2\pi, \phi > 0$), $R_i'$ is large since the wave shear becomes small, having linear dependence on $\sigma$ which approaches zero near the stability boundary. The distance of propagation away from the slope in the up-slope flow for waves formed with $\phi_0 < 0$, decreases as $\phi_0$ increases from $-0.16$ to $-0.04$, $Kd$ decreasing from 0.08 to 0.003. $Kd$ reaches 0.18 for waves generated at $\phi_0 = 0.08$ which propagate to $\phi = 0.8$.

## 5. Discussion

The orientation, $\beta$, of the small-scale waves at A (figure 2) lies between 125° and 165°, the most intense waves having $\beta$ near 150°, whilst those at B have an orientation near 360°. These are consistent with the orientations of waves predicted to have the greatest amplitude (figure 6*b*). Both types of waves can be detected at C where the flow is up-slope.

Waves at A have a length of about 0.8 cm ($\gamma = 11$) whilst those at B have a length of 0.4 cm ($\gamma = 22$), somewhat less than those the waves predicted in figure 6 to have the largest amplitude. However, within about one-quarter of the long-wave period, the short waves can be detected some 2.5 cm from the grid, giving $Kd \approx 0.65$, in excess of the values predicted in §4. It seems unlikely that the waves with near-horizontal phase lines ($\beta$ near 0, $\pi$ or $2\pi$) may contribute to mixing since $R_i'$ is large (see figure 6*c*), and indeed no mixing appears to be associated with these waves in the experiments. The effect of viscosity on these very small (and hence low-Reynolds-number) waves may both suppress them (leading to the loss of waves with large $\gamma$) and reduce any tendency for them to promote turbulence. The near-vertical waves predicted to have large amplitude (figure 6*b*, $\beta$ near $\frac{3}{2}\pi$, $\phi = 0.8$) are not observed. It must be recalled, however, that the shadowgraph is sensitive to gradients in refractive index, and that the magnitude of the second derivative of density will provide a better indication of the presence of waves. This will be large if both the wave amplitude *and* the square of the wavenumber is large. Whilst $a/a_0$ is predicted to be fairly large near $\beta = \frac{3}{2}\pi$ (figure 6*b*), $\gamma$ is not particularly large (figure 6*d*), and it seems likely that for this reason the waves here are not detectable.

We set out in §3.1 to provide a plausible explanation of the fine-scale distortion of the density field during certain parts of the $M_2$ baroclinic tidal cycle on the slope of the Porcupine Bank. Whilst some of the predictions of the theory have been verified in the simple laboratory experiment, a direct comparison with the measurements in the ocean is not possible because of the absence of information about the scale of variation of the bottom topography. The variation in the amplitude of the fluctuations during the tidal cycle of 10–12 m, their phase relationship with the $M_2$ tide, and the scale of separation of the layers (20–50 m) in comparison with the $M_2$ wavelength (about 1000 m), giving $\gamma = 20$ to 50, are, however, reasonably consistent with the predictions in figures 4 and 5 for the up-slope flow near $\phi = 0.8$. It should be noticed that these waves have $\frac{3}{2}\pi < \beta < 2\pi$, so they have an upward phase speed and a downward group velocity, both *relative* to the fluid. Their phase configuration is, however, such that, as they are advected by the long-wave flow, a downward phase propagation would be observed at a fixed position (see figure 3*c*). Although

waves may be large near a caustic (e.g. as in figure 4), the long-wave flow here is down-slope ($\phi < 0$) whereas the observed waves occur primarily during phases of up-slope flow. Possibly the conditions are closer to those with $\gamma_1 = 8$ (figure 5) when there is no caustic. As was found in the experiments, the distance from the slope at which short internal waves were observed (up to 82 m off the Porcupine Bank) exceeds that predicted (only some 25 m), and this points to shortcomings of the theory.

One severe approximation is that the short waves in §2.2 are supposed to be of small amplitude. Baines (1971*a*) in particular has pointed to the fact that 'linearized theory, although instructive and quite probably very useful, is really on the fringes of the phenomenon', in the sense that nonlinear effects are likely to be important. The considerable amplifications of waves predicted in figures 4–6 is an indication that this is so. In considering an internal wave flowing over sloping sinusoidal topography Baines found that two new waves were generated by reflection having sum and difference wavenumbers of what we have called the long wave and the bottom topography. The long-wave assumption made here implies that the only waves generated are those that are locally 'standing' in the current produced by the long wave on the slope, and that these have an along-slope wavenumber identical to that of the topography. Two new wave packets are indeed formed (as in figure 2), but with varying $\beta_0$ depending on $\phi_0$. We have neglected the currents associated with the barotropic component of the $M_2$ tide as well as the mean flow, and the effects of along-slope topography and the internal waves which it may cause. These are likely to be important, and should be considered in further studies which will require careful use of the dispersion relation (see the Appendix) and evaluation of wave energy. Whilst we have not demonstrated that the descending layered structure seen in the high-resolution measurement off the Porcupine Bank is indeed produced locally as a consequence of the baroclinic tidal flow over topography, we have shown that small-scale topography can play an important role in promoting conditions for strong wave–wave interactions at ocean boundaries.

The processes dominating ocean boundary mixing, those which must be accounted for in deciding whether it is of basin-wide importance, are far from clear. They probably depend on local topography, currents, atmospheric forcing and stratification, and merit a far more intensive and detailed study than has yet been attempted. Several processes involving internal waves are now known, reflection at near-critical angles, incident and reflected wave interaction at certain bottom slopes, and the wave–topography interactions and subsequent wave distortion described here. In practice other wave effects, such as parametric instability and slow modulation of internal waves by larger-scale slope and Kelvin waves, may have to be accounted for. All we have done is to point to a process that may, or may not, contribute significantly but which appears to account for some of the observations.

Mr Martin White made the laboratory experiment and measurements described in §§3.2 and 5, and provided figure 2. I am most grateful for his cooperation.

## Appendix. Internal waves with a wavenumber in the $y$-direction

A solution of the linearized equation of motion with linear density gradients in the $x$- and $z$-directions may be found proportional to $\exp \mathrm{i}(lx+my+nz-\sigma t)$ with a dispersion relation (corresponding to (8)) of the form

$$\sigma^3(l^2+m^2+n^2) = \sigma[(l^2+m^2)N_z^2 - lmN_x^2 + n^2f^2] - \mathrm{i}N_x^2 fmn.$$

In general, this has imaginary roots corresponding to growing disturbances. For example, in the case $l = 0$, the short waves described by this relation have a wavenumber at right angles to that of the long wave, and writing $\sigma = \mathrm{i}\sigma'$ and $\tan\beta = m/n$ we find

$$\sigma'^3 + \sigma'(N_z^2 \sin^2\beta + f^2\cos^2\beta) - N_x^2 f \sin\beta\cos\beta = 0,$$

which has one real root which is $>0$ if $N_x^2 f \sin\beta\cos\beta > 0$, giving an unstable, exponentially growing, solution.

## REFERENCES


Armi, L. 1979 Effects of variations in eddy diffusivity on property distributions in the oceans. *J. Mar. Res.* **37**, 515–530.

Baines, P. G. 1971*a* The reflexion of internal/inertial waves from bumpy surfaces. *J. Fluid Mech.* **46**, 273–291.

Baines, P. G. 1971*b* The reflexion of internal/inertial waves from bumpy surfaces. Part 2. Split reflexion and diffraction. *J. Fluid Mech.* **49**, 113–131.

Bell, T. H. 1975 Topographically generated internal waves in the open ocean. *J. Geophys. Res.* **80**, 320–327.

Booker, J. R. & Bretherton, F. P. 1967 Critical layer for internal gravity waves in a shear flow. *J. Fluid Mech.* **27**, 513–539.

Bretherton, F. P. 1966 The propagation of groups of internal waves in a shear flow. *Q. J. R. Met. Soc.* **92**, 466–480.

Bretherton, F. P. & Garrett, C. J. R. 1968 Wavetrains in inhomogeneous moving media. *Proc. R. Soc. Lond.* A **302**, 529–554.

Broutman, D. 1984 The focussing of short internal waves by an inertial wave. *Geophys. Astrophys. Fluid Dyn.* **30**, 199–225.

Broutman, D. 1986 On internal wave caustics. *J. Phys. Oceanogr.* **16**, 1625–1635.

Broutman, D. & Grimshaw, R. 1988 The energetics of the interaction between short small-amplitude internal waves and near inertial waves. *J. Fluid Mech.* **196**, 93–106.

Broutman, D. & Young, W. R. 1986 On the interaction of small-scale oceanic internal waves with near-inertial waves. *J. Fluid Mech.* **166**, 341–358.

Cacchione, D. & Wunsch, C. 1974 Experimental study of internal waves over a slope. *J. Fluid Mech.* **66**, 223–240.

Drazin, P. G. 1977 On the instability of an internal gravity wave. *Proc. R. Soc. Lond.* A **356**, 411–432.

Eriksen, C. C. 1982 Observations of internal wave reflexion off sloping bottoms. *J. Geophys. Res.* **87**, 525–538.

Eriksen, C. C. 1985 Implications of ocean bottom reflexion for internal wave spectra and mixing. *J. Phys. Oceanogr.* **15**, 1145–1159.

Garrett, C. J. R. 1967 The adiabatic invariant for wave propagation in a non-uniform moving medium. *Proc. R. Soc. Lond.* A **299**, 26–27.

Garrett, C. & Gilbert, D. 1988 Estimates of vertical mixing by internal waves reflected off a sloping bottom. In *Small-Scale Turbulence and Mixing in the Ocean* (ed. J. C. J. Nihoul & B. M. Jamart), pp. 405–424. Elsevier.

Gill, A. E. 1982 *Atmosphere–Ocean Dynamics*. Academic Press. 662 pp.

Henyey, F. S., Creamer, D. B., Dysthe, K. B., Schult, R. L. & Wright, J. A. 1988 The energy and action of small waves riding on large waves. *J. Fluid Mech.* **189**, 443–462.

Klostermeyer, J. 1982 On the parametric instabilities of finite-amplitude internal gravity waves. *J. Fluid Mech.* **119**, 367–377.

Koop, C. G. 1981 A preliminary investigation of the interaction of internal gravity waves with a steady shearing motion. *J. Fluid Mech.* **113**, 347–386.

Koop, C. G. & McGee, B. 1986 Measurements of internal gravity waves in a continuously stratified fluid. *J. Fluid Mech.* **172**, 453–480.

LAZIER, J. R. N. 1973 Temporal changes in some fresh water temperature structures. *J. Phys. Oceanogr.* **3**, 226–229.

LONGUET-HIGGINS, M. S. 1987 The propagation of short surface waves on longer gravity waves. *J. Fluid Mech.* **177**, 293–306.

MIED, R. P. 1976 The occurrence of parametric instabilities in finite-amplitude internal gravity waves. *J. Fluid Mech.* **78**, 763–784.

MIED, R. P. & DUGAN, J. P. 1976 Internal wave reflexion from a sinusoidally corrugated surface. *J. Fluid Mech.* **76**, 259–272.

MÜLLER, M. R. & KARLSSON, S. K. F. 1981 Experiments on the propagation of composite internal wave trains. *Phys. Fluids* **24**, 1937–1943.

MUNK, W. H. 1966 Abyssal recipes. *Deep-Sea Res.* **13**, 707–730.

THORPE, S. A. 1984 A laboratory study of stratified accelerating flow over a rough boundary. *J. Fluid Mech.* **138**, 185–196.

THORPE, S. A. 1987*a* On the reflexion of a train of finite-amplitude internal waves from a uniform slope. *J. Fluid Mech.* **178**, 279–302.

THORPE, S. A. 1987*b* Current and temperature variability on the continental slope. *Phil. Trans. R. Soc. Lond.* A**323**, 471–517.

THORPE, S. A. 1988 Benthic boundary layers on slopes. In *Small-scale Turbulence and Mixing in the Ocean* (ed. J. C. J. Nihoul & B. M. Jamart), pp. 425–434. Elsevier.

THORPE, S. A. & HAINES, A. P. 1987 A note on observations of wave reflection on a 20° slope. Appendix to S. A. Thorpe, **178**, 279.

WEATHERLEY, G. L. & MARTIN, P. J. 1978 On the structure and dynamics of the oceanic bottom boundary layer. *J. Phys. Oceanogr.* **8**, 557–570.